

Subdiffraction Far-Field Imaging of Luminescent Single-Walled Carbon Nanotubes

Laurent Cognet,^{*,†,‡} Dmitri A. Tsyboulski,[†] and R. Bruce Weisman^{*,†}

Department of Chemistry, Richard E. Smalley Institute for Nanoscale Science and Technology, and Center for Biological and Environmental Nanotechnology, Rice University, 6100 Main Street, Houston, Texas 77005, and Centre de Physique Moléculaire Optique et Hertzienne, Université Bordeaux 1, and CNRS, Talence, F-33405 France

Received October 2, 2007; Revised Manuscript Received December 27, 2007

ABSTRACT

Far-field near-infrared fluorescence microscopy of single-walled carbon nanotubes (SWNTs) has been hampered by the diffraction limit to resolution. A new analysis method is presented that allows subwavelength ($<\lambda/10$) mapping of single-molecule chemical reaction sites on semiconducting SWNTs, enabling precise localization of excitonic luminescence regions along the nanotube axis through a nonperturbing, far-field optical measurement. This method is applied to reveal the subdiffraction lengths, curvatures, and defects of luminescent SWNTs in unprecedented detail.

Optical excitation of semiconducting single-walled carbon nanotubes (SWNTs) leads to near-infrared luminescence through radiative recombination of excitons.^{1,2} This emission allows the detection of individual nanotubes in a range of physical, chemical, and biological environments through fluorescence microscopy.^{3–8} However, spatial resolution in the far field is limited by diffraction to a value much larger than the ~ 90 nm exciton excursion range at room temperature, which defines an important scale for elementary photophysical processes.⁷ Although blinking has been observed for some nanotubes dried on a surface,⁹ photoluminescence of SWNTs in aqueous suspensions is generally reported to be stable.^{3,7} We show, however, that the luminescence of isolated SWNTs suspended in sodium dodecylbenzenesulfonate (SDBS) displays unceasing intermittency in controlled acidic environments, due to localized individual protonation/deprotonation reactions. We isolate these sudden changes in luminescence intensity by computing differential images between consecutive video microscopy frames. Knowledge of the microscope's point spread function is then used to extract the positions of the localized single-molecule reaction sites with subwavelength precision. When the positions of multiple reaction sites are combined, they reveal a high-resolution map of the nanotube's luminescent regions.

We prepared samples containing highly luminescent and relatively long nanotubes by dispersing raw HiPco SWNTs in aqueous SDBS surfactant using very brief tip ultrasonication.⁵ To immobilize the nanotubes while keeping them in aqueous environments, the dispersed tubes were diluted and mixed in a melted 5% agarose gel preparation. The pH in the samples was adjusted using sulfuric acid and kept constant. A drop of the melted mixture was then sandwiched between a glass slide and a cover slip and sealed with silicone grease to prevent drying. The samples were mounted onto an inverted microscope (Nikon TE-2000U) equipped with a 60 \times objective (NA = 1.4, Nikon). An additional 1.5 \times magnification was used such that a single pixel width corresponded to 335 nm. Samples were continuously excited from above by a 658 nm diode laser beam. The infrared photoluminescence emitted by the SWNTs passed through long-pass infrared filters (FEL 946, Thorlabs) and was detected by a liquid-nitrogen-cooled 16-bit InGaAs 2D array (OMA-V 2D, Princeton Instruments). Laser intensities were kept below 1 kW/cm² to avoid exciton–exciton annihilation effects¹⁰ that would shorten the exciton excursion range. We recorded luminescence image sequences with an integration time of 50 ms and a readout dead time of 4 ms for up to 10 000 consecutive frames. A second port of the microscope was fiber-optically coupled to a near-IR spectrograph with a 512-channel InGaAs detector array for recording SWNT emission spectra. Both spatially unresolved and micrometers-long SWNTs were identified in the near-IR photoluminescence

* Corresponding authors. E-mail: lcognet@u-bordeaux1.fr; weisman@rice.edu.

[†] Rice University.

[‡] Université Bordeaux.

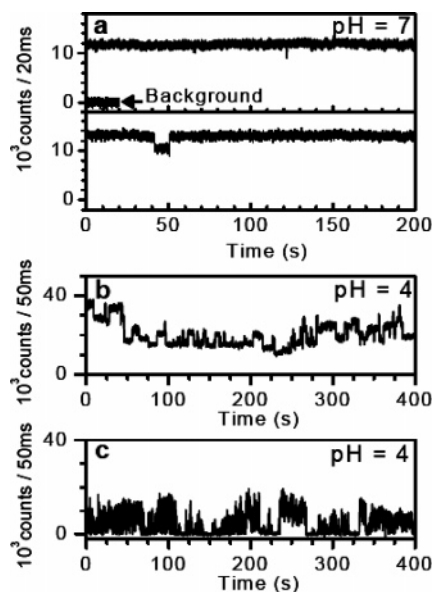


Figure 1. Acid-induced photoluminescence intermittency of diffraction-limited segments of individual SWNTs immobilized in gels. (a) Emission intensity from two segments of the same nanotube at pH 7. (b and c) Emission intensity from different nanotubes at pH 4.

(PL) images. The (n,m) identity of an individual SWNT was deduced from the peak wavelength of its narrow Lorentzian emission spectrum.¹¹

The pH in the sample gels was held constant within the range from 4 to 8 (± 0.5). For pH values above 7, most of the nanotubes displayed highly stable PL for tens of minutes under continuous laser illumination at intensities near 900 W/cm². At pH 7, some SWNT segments showed occasional PL intensity steps that were highly localized (Figure 1a). At pH 4, these local intensity changes became very frequent (Figure 1b). Furthermore, a fraction of the SWNTs that were shorter than the diffraction limit displayed complete on/off blinking behavior (Figure 1c). We have previously reported the transient occurrence of intensity steps as the PL of individual SWNTs was quenched during acidification.⁷ We attributed such steps to single protonation/deprotonation reactions at the nanotube side wall. In the present work, the observation of continuing PL intermittency at constant pH confirms that single protonation/deprotonation reactions can occur repeatedly under steady-state conditions, supporting the proposed mechanism for acid PL quenching. This mechanism is thought to involve the injection of a hole into the nanotube π -system near the protonation site.^{1,12,13} If an exciton encounters such a chemically induced hole before it recombines radiatively, then the exciton's PL is quenched efficiently through nonradiative Auger processes.¹⁴ In such a scheme and for nanotubes that are longer than the ~ 90 nm exciton excursion range (Λ),⁷ only a fraction of the excitons generated within a diffraction-limited segment ($\lambda/2 \sim 600$ nm) would be quenched by a single protonation-induced hole. Subsequent deprotonation would remove the quenching site and restore the original PL intensity. In this model, the complete on/off blinking behavior displayed in Figure 1c is expected only for nanotubes with lengths less

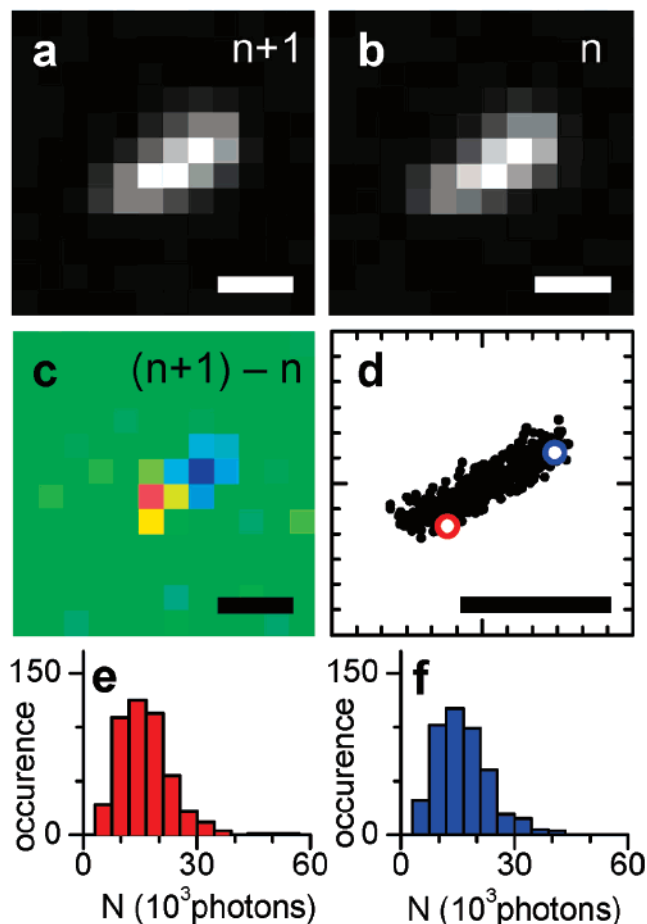


Figure 2. Generation of single-molecule reaction site map for a SWNT at pH 4. (a and b) Consecutive 50 ms photoluminescence image frames before processing. (c) The color-coded difference image between frames shown in a and b revealing the presence of one positive (red) and one negative (blue) intermittency spot (i-spot). (d) Positions of the two i-spots (red and blue open circles) deduced from 2D Gaussian fitting as described in the text. Black symbols show the positions of all other intermittency spots found from the 10 000 frame video recording. (e and f) Distributions of the spatially integrated signal amplitudes in the positive and negative i-spots, respectively, obtained by the fits. All scale bars are 1 μ m.

than Λ . More generally, PL intermittency would originate from the on/off blinking of nanotube segments whose lengths are directly related to Λ , which is well below the diffraction limit and therefore not directly accessible through conventional microscopy. We present below a new analysis method that retrieves with subdiffraction resolution the locations of these blinking segments created by stochastic single-molecule reactions.

We first computed differential images of the differences between successive near-IR image frames (see Figure 2 a–c). Positive and negative intermittency spots (i-spots) became apparent in these differential images, reflecting the sudden PL changes occurring along the nanotubes at pH 4 (Figure 2c). The majority of the i-spots are diffraction-limited (2 pixels correspond to 670 nm in Figure 2c), as is consistent with a PL wavelength much greater than Λ , and they appear mainly uncorrelated in time and space. We then statistically fit each i-spot spatial distribution to a Gaussian approximating the true point-spread function. These fits retrieve the

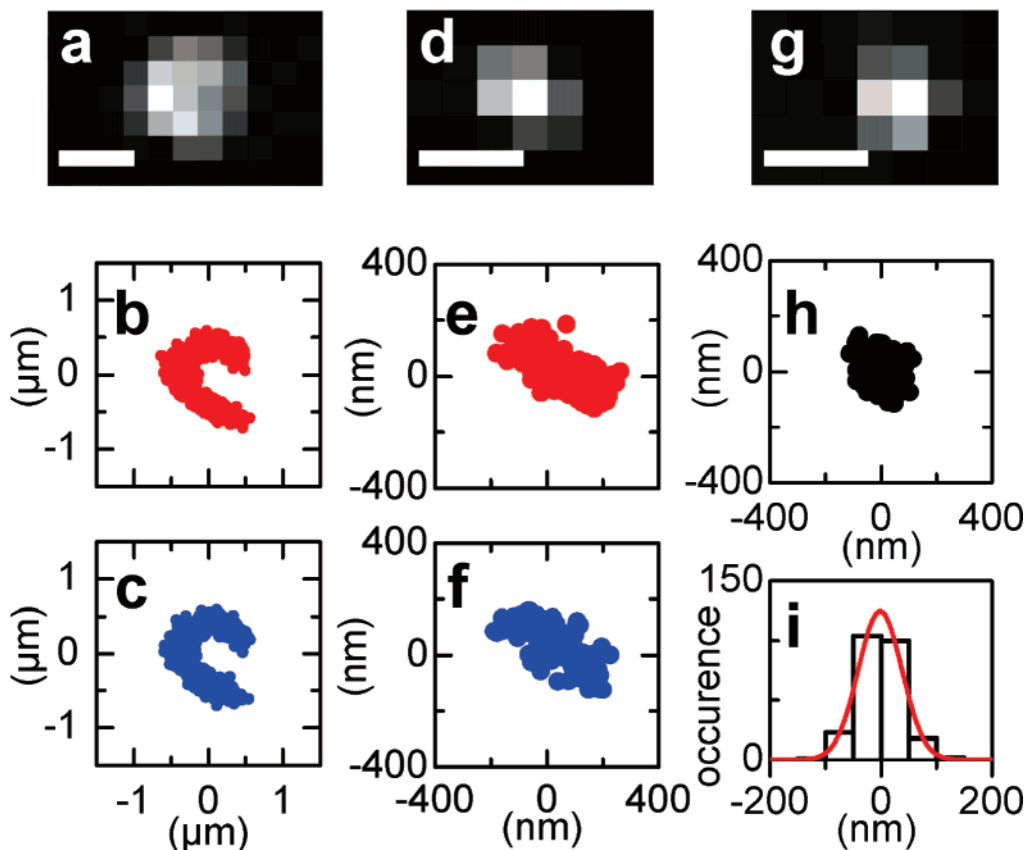


Figure 3. Subwavelength determination of morphology and length of individual SWNTs. (a, d, and g) Luminescence images of three nanotubes. Scale bars are $1\ \mu\text{m}$. (b and c) Maps constructed from positions of positive and negative i-spots, respectively, for the nanotube shown in a. (e and f) Maps constructed from positions of positive and negative i-spots, respectively, for the nanotube shown in d. (h) Map constructed from both positive and negative i-spots for the nanotube shown in g. (i) Distribution of i-spot locations along the major axis of the nanotube mapped in h.

locations of the i-spot centroids with subwavelength accuracy and provide their spatially integrated amplitudes, corresponding to the change in number of detected photons, N .^{15–17} As an example, the red and blue circles on Figure 2d show the positions of the two i-spots in Figure 2c. For this nanotube, we have analyzed 453 negative and 471 positive i-spots and plotted their locations as black points in Figure 2d. Figure 2e and f show the distributions of their amplitudes, N , which can be seen to be equivalent and mainly unimodal. This confirms that single protonation and deprotonation reactions dominate the PL intermittency because multistep events would lead to broad, multimodal distributions. If background noise can be neglected relative to N , then the error in the fitted position can be approximated by $\sigma_{x,y} \sim s/N^{1/2}$, where s is the standard deviation of the fitting Gaussian ($\sim 650\ \text{nm}$ for a PL wavelength of $1300\ \text{nm}$).^{16,18} Given that each i-spot typically represents a change of more than 10^4 photons, a resolution below $10\ \text{nm}$ would be expected. However, the measured transverse resolution was $\sim 40\ \text{nm}$ for the (9,2) SWNT presented in Figure 2. This indicates that our NIR detector is not operating in the shot-noise limited regime. The minimal dimension that will be resolved parallel to the nanotube axis in our experiments is given by the convolution of the transverse resolution with Λ . This result is approximately $100\ \text{nm}$, a value less than $\lambda/10$. Figure 2d shows the map of the nanotube constructed by compiling 924

i-spots. This image illustrates that our method can provide a high-density map of reaction events (typically $\sim 1000/\mu\text{m}$) even within diffraction-limited regions.

The top row in Figure 3 presents fluorescence images of three different SWNTs. The shape of the one in Figure 3a is not evident, and the two others, which have lengths shorter than the diffraction limit, at first appear identical. However, the i-spot maps shown in frames b, c, e, f, and h reveal a distinct “C” shape for the first one (likely reflecting high stress exerted during preparation of the gel sample) and show that the lengths of the two other ones are very different. More precisely, the length of the tube presented in Figure 3d is slightly below the diffraction limit ($\sim 500\ \text{nm}$, Figure 3e and f) and its orientation is also unambiguously revealed. We confirmed this orientation using linearly polarized excitation light.⁵ In contrast, the length of the tube presented in Figure 3g is much shorter ($100\ \text{nm}$ full width at half-maximum (fwhm)), as can be seen in Figure 3h and i). This i-spot map illustrates the axial resolution limit imposed by Λ . Interestingly, the complete on- and off-blinking behavior presented in Figure 1d was measured from this SWNT, exactly as expected for such short nanotubes.

The SWNT length determination described here reveals only nanotube segments in which excitons recombine radiatively. If the nanotube ends act as quenching sites, then excitons created within a distance of $\sim \Lambda/2$ of the ends will

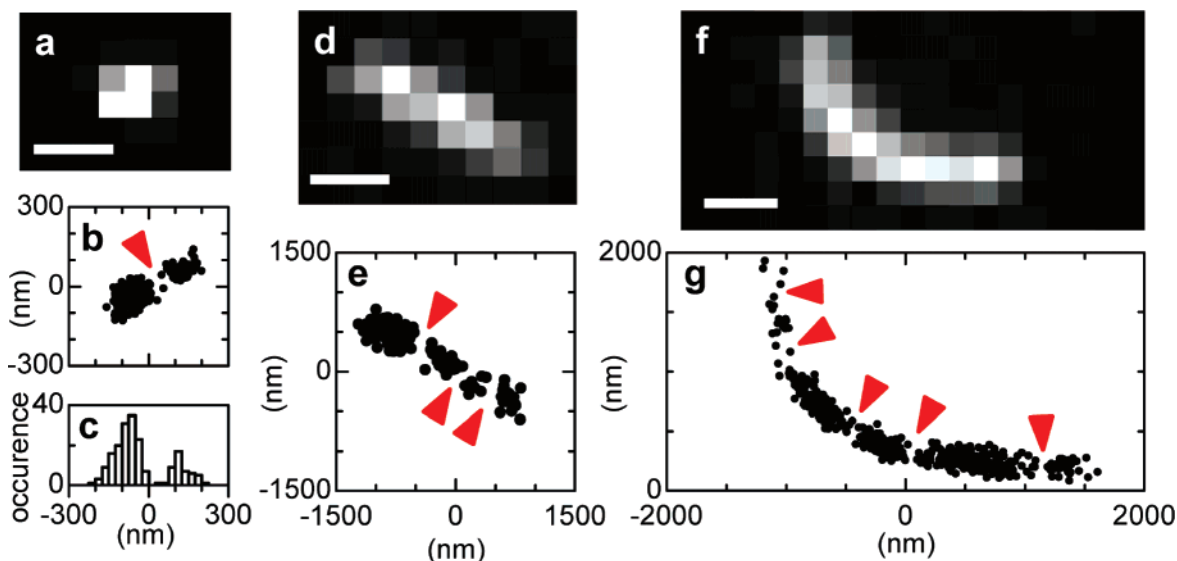


Figure 4. Subwavelength determination of luminescence defects in individual SWNTs. (a–c) Luminescence image, i-spot map, and distribution of i-spot locations along the major axis of one nanotube. (d and f) Luminescence images of two different nanotubes in the presence of 10 nm gold nanoparticles. (e and g) i-spot maps corresponding to the nanotubes shown in d and f. Triangles indicate the locations of luminescence defects. All scale bars are 1 μm .

not recombine radiatively. The apparent nanotube length deduced from the i-spot map would then be shorter than the physical length by Λ . Additional studies will be needed to confirm this assumption. Nevertheless, our single-particle study provides the first direct evidence that very short (~ 100 nm) segments within nanotubes can luminesce efficiently.

The i-spot maps corresponding to protonations or deprotonations for the same nanotubes are indistinguishable (Figure 3b and c and 3e and f). For most SWNTs that appear uniformly bright, we find i-spots that are uniformly distributed along the nanotube lengths (Figure 2 and 3). On occasion, however, the maps reveal the presence of a short subwavelength segment (~ 100 nm) in which no i-spots are detected (Figure 4a–c), even though the nanotube’s near-IR fluorescence image appears entirely uniform. We hypothesize that such segments originate from isolated permanent physical or chemical defects in the nanotube that quench the excitonic PL within a range of Λ . Our samples also contain some long (multimicrometer) nanotubes that show nonuniform images in conventional fluorescence microscopy.¹⁹ However, these SWNTs are difficult to study using i-spot mapping because of their weak emission within regions of high defect density. In an attempt to control the number of quenching defects, we mixed a high concentration of 10 nm gold nanoparticles ($\sim 1\text{--}10$ particles per μm^3) with the nanotubes during gel preparation to act as extrinsic local quenching sites.²⁰ The density was, however, kept low enough to ensure that the induced defects remained invisible in normal fluorescence imaging. Bright nanotubes with relatively uniform emission profiles were then imaged at pH 4, as described above. Analysis of their i-spot maps revealed that a large fraction of nanotubes exposed to gold nanoparticles displayed similar blank sections (Figure 4d–g), which we interpret as regions of exciton quenching caused by nanoparticles trapped by the gel in the vicinity of the nanotubes. This result shows that our i-spot mapping method

can reveal and locate quenching perturbations within a nanotube with subwavelength resolution.

Recently, several ensemble and single-molecule approaches have been developed to image features below the diffraction limit.²¹ The method presented here is conceptually related to those single-molecule methods that extract the positions of luminescent objects separated by only a few nanometers. Small numbers of fluorophores or quantum dots located within the diffraction limit were resolved by using their photobleaching^{22,23} or blinking properties.²⁴ In order to locate single molecules at higher densities, Betzig et al. recently used serial photoactivation and subsequent bleaching of numerous sparse subsets of photoactivatable fluorescent protein molecules.²⁵ Zhuang et al. developed a stochastic optical reconstruction microscopy scheme (STORM) that retrieves the position of pairs of molecules that are switched on and off using different excitation wavelengths.^{26,27} By comparison, in our method the PL intermittency produced by single-molecule reactions is analyzed to reveal intranotube features with subwavelength resolution. This allows fine far-field measurements of nanotube lengths, curvatures, and orientations. In addition, our method can map the small nonemissive regions caused by permanent defects or chemical derivatization of a nanotube side wall. It will thereby allow measurement of the density and spatial distribution of these “dark” regions in greater detail, allowing improved insight into the processes that generate exciton quenching sites and their abundance in different samples.

Acknowledgment. This work was supported by grants from the NSF Center for Biological and Environmental Nanotechnology (EEC-0647452), the Welch Foundation (C-0807), and Applied NanoFluorescence, LLC. We are also grateful to S. W. Casscells, III and J. L. Conyers (Univ. of Texas Health Science Center, Houston) for instrumentation support. L.C. thanks the Fulbright Foundation and the DGA

(ERE060016) for financial support, and D.A.T. thanks the Welch Foundation for a postdoctoral fellowship (L-C-0004).

References

- (1) O'Connell, M.; Bachilo, S. M.; Huffman, C. B.; Moore, V.; Strano, M. S.; Haroz, E.; Rialon, K.; Boul, P. J.; Noon, W. H.; Kittrell, C.; Ma, J.; Hauge, R. H.; Weisman, R. B.; Smalley, R. E. *Science* **2002**, *297*, 593–596.
- (2) Wang, F.; Dukovic, G.; Brus, L. E.; Heinz, T. F. *Science* **2005**, *308*, 838–841.
- (3) Hartschuh, A.; Pedrosa, H. N.; Novotny, L.; Krauss, T. D. *Science* **2003**, *301*, 1354–1356.
- (4) Lefebvre, J.; Fraser, J. M.; Finnie, P.; Homma, Y. *Phys. Rev. B* **2004**, *69*, 075403–1–075403–5.
- (5) Tsyboulski, D. A.; Bachilo, S. M.; Weisman, R. B. *Nano Lett.* **2005**, *5*, 975–979.
- (6) Cherukuri, P.; Gannon, C. J.; Leeuw, T. K.; Schmidt, H. K.; Smalley, R. E.; Curley, S. A.; Weisman, R. B. *Proc. Natl. Acad. Sci. U.S.A.* **2006**, *103*, 18882–18886.
- (7) Cognet, L.; Tsyboulski, D.; Rocha, J.-D. R.; Doyle, C. D.; Tour, J. M.; Weisman, R. B. *Science* **2007**, *316*, 1465–1468.
- (8) Leeuw, T. K.; Reith, R. M.; Simonette, R. A.; Harden, M.; Cherukuri, P.; Tsyboulski, D. A.; Beckingham, K. M.; Weisman, R. B. *Nano Lett.* **2007**, *7*, 2650–2654.
- (9) Matsuda, K.; Kanemitsu, Y.; Irie, K.; Saiki, T.; Someya, T.; Miyauchi, Y.; Maryama, S. *Appl. Phys. Lett.* **2005**, *86*, 12316–1–12316–3.
- (10) Ma, Y.-Z.; Valkunas, L.; Dexheimer, S. L.; Bachilo, S. M.; Fleming, G. R. *Phys. Rev. Lett.* **2005**, *94*, 157402–1–157402–4.
- (11) Weisman, R. B.; Bachilo, S. M. *Nano Lett.* **2003**, *3*, 1235–1238.
- (12) Strano, M. S.; Huffman, C. B.; Moore, V. C.; O'Connell, M. J.; Haroz, E. H.; Hubbard, J.; Miller, M.; Rialon, K.; Kittrell, C.; Ramesh, S.; Hauge, R. H.; Smalley, R. E. *J. Phys. Chem. B* **2003**, *107*, 6979–6985.
- (13) Dukovic, G.; White, B. E.; Zhou, Z. Y.; Wang, F.; Jockusch, S.; Steigerwald, M. L.; Heinz, T. F.; Friesner, R. A.; Turro, N. J.; Brus, L. E. *J. Am. Chem. Soc.* **2004**, *126*, 15269–15276.
- (14) Wang, F.; Dukovic, G.; Knoesel, E.; Brus, L. E.; Heinz, T. F. *Phys. Rev. B* **2004**, *70*, 241403(R)-1–241403(R)-4.
- (15) Schmidt, T.; Schuetz, G. J.; Baumgartner, W.; Gruber, H. J.; Schindler, H. *Proc. Natl. Acad. Sci. U.S.A.* **1996**, *93*, 2926–2929.
- (16) Cheezum, M. K.; Walker, W. F.; Guilford, W. H. *Biophys. J.* **2001**, *81*, 2378–2388.
- (17) Tardin, C.; Cognet, L.; Bats, C.; Lounis, B.; Choquet, D. *EMBO J.* **2003**, *22*, 4656–4665.
- (18) Thompson, R. E.; Larson, D. R.; Webb, W. W. *Biophys. J.* **2002**, *82*, 2775–2783.
- (19) Tsyboulski, D.; Rocha, J.-D. R.; Bachilo, S. M.; Cognet, L.; Weisman, R. B. *Nano Lett.* **2007**, *7*, 3080–3085.
- (20) Nikoobakht, B.; Burda, C.; Braun, M.; Hun, M.; El-Sayed, M. A. *Photochem. Photobiol.* **2002**, *75*, 591–597.
- (21) Hell, S. W. *Science* **2007**, *316*, 1153–1158.
- (22) Gordon, M. P.; Ha, T.; Selvin, P. R. *Proc. Natl. Acad. Sci. U.S.A.* **2004**, *101*, 6462–6465.
- (23) Qu, X.; Wu, D.; Mets, L.; Scherer, N. F. *Proc. Natl. Acad. Sci. U.S.A.* **2004**, *101*, 11303.
- (24) Lidke, K. A.; Rieger, B.; Jovin, T. M.; Heintzmann, R. *Opt. Express* **2005**, *13*, 7052–7062.
- (25) Betzig, E.; Patterson, G. H.; Sougrat, R.; Lindwasser, O. W.; Olenych, S.; Bonifacino, J. S.; Davidson, M. W.; Lippincott-Schwartz, J.; Hess, H. R. *Science* **2006**, *313*, 1642–1645.
- (26) Bates, M.; Blosser, T. R.; Zhuang, X. W. *Phys. Rev. Lett.* **2005**, *94*, 108101–1–108101–4.
- (27) Rust, M. J.; Bates, M.; Zhuang, X. *Nat. Methods* **2006**, *3*, 793–795.

NL0725300